Electrically reconfigurable silicon microring resonator-based filter with waveguide-coupled feedback

Linjie Zhou and Andrew W. Poon

Photonic Device Laboratory, Department of Electronic and Computer Engineering, The Hong Kong University of Science and Technology, Clear Water Bay, Hong Kong SAR, China
eeawpoon@ust.hk

Abstract: We demonstrate an electrically reconfigurable silicon microring resonator-based filter with waveguide-coupled feedback. Our experiments and scattering-matrix-based modeling show that the resonance wavelengths, extinction ratios, and line shapes depend on the feedback coupling and can be controllably tuned by means of carrier injection to the feedback-waveguide. We also demonstrate nearly uniform resonance line shapes over multiple free-spectral ranges by nearly phase-matching the feedback and the microring.

OCIS codes: (130.3120) Integrated optics devices; (230.5750) Resonators; (260.5740) Resonance.

References and links

1. R. Soref, "The past, present, and future of silicon photonics," IEEE J. of Sel. Top. Quantum Electron. **12**, 1678-1687 (2006).
2. N. Izhaky, M. T. Morse, S. Koehl, O. Cohen, D. Rubin, A. Barkai, G. Sarid, R. Cohen, and M. J. Paniccia, "Development of CMOS-compatible integrated silicon photonics devices," IEEE J. of Sel. Top. Quantum Electron. **12**, 1688-1698 (2006).
3. B. Jalali, "Silicon photonics," J. Lightwave Technol. **24**, 4600-4615 (2006).
4. G. Lenz and C. K. Madsen, "General optical all-pass filter structures for dispersion control in WDM systems," J. Lightwave Technol. **17**, 1248-1254 (1999).
5. G. T. Paloczi, Y. Huang, A. Yariv and S. Mookherjea, "Polymeric Mach-Zehnder interferometer using serially coupled microring resonators," Opt. Express **11**, 2666-2671 (2003).
6. W. Green, R. Lee, G. DeRose, A. Scherer, and A. Yariv, "Hybrid InGaAsP-InP Mach-Zehnder Racetrack Resonator for Thermooptic Switching and Coupling Control," Opt. Express **13**, 1651-1659 (2005).
7. S. Mookherjea, "Mode cycling in microring optical resonators," Opt. Lett. **30**, 2751-2753 (2005).
8. M. R. Watts, T. Barwicz, M. Popovic, P. T. Rakich, L. Socci, E. P. Ippen, H. I. Smith, and F. Kaertner, "Microring-resonator filter with doubled free-spectral-range by two-point coupling," in proceedings of Conference on Lasers and Electro-Optics (Optical Society of America, Washington, DC, 2005), **CMP3**.
9. C. Li, L. Zhou, and A. W. Poon, "Silicon microring carrier-injection-based modulators/switches with tunable extinction ratios and OR-logic switching by using waveguide cross-coupling," Opt. Express **15**, 5069-5076 (2007).
10. R. A. Soref and B. R. Bennett, "Electrooptical effects in silicon", IEEE J. Quantum Electron **23**, 123-129 (1987).
11. B. E. A. Saleh and M. C. Teich, *Fundamentals of Photonics*, 2nd edition, (John Wiley & Sons, 2007), Chap. 8.
12. L. Zhou and A. W. Poon, "Fano resonance-based electrically reconfigurable add-drop filters in silicon microring resonator-coupled Mach-Zehnder interferometers," Opt. Lett. **32**, 781-783 (2007).
13. U. Fano, "Effect of configuration interaction on intensities and phase shifts," Phys. Rev. **124**, 1866-1878 (1961).

1. Introduction

Silicon microring resonators are promising building blocks for highly compact optoelectronic integrated circuits (OEICs) that are compatible with mature silicon microelectronics [1-3]. Silicon microring OEICs are potentially relevant to a wide scope of applications including telecommunications, computer interconnects, and biochemical sensing. While conventional

#83924 - $15.00 USD Received 7 Jun 2007; revised 8 Jul 2007; accepted 9 Jul 2007; published 11 Jul 2007

microring-based notch and add-drop filters comprise simple waveguide coupling to the microring resonator, in which resonance dips appear in the throughput-port and resonance peaks appear in the drop-port, it is conceivable that resonance control and thereby advanced wavelength-agile functionalities can be attained by means of external feedback. Several research groups [4-9] have proposed and investigated such interferometric approach to resonance control by means of waveguide cross-coupling to a microresonator, in which a cross-coupled waveguide provides an external feedback to the microresonator. Various resonance characteristics and functionalities for such feedback-coupled microresonators have been studied including transmission dispersion [4], interferometers with slow-light [5], resonance extinction ratio (ER) control [6], clockwise- and counterclockwise-traveling-wave modes mutual coupling [7], resonance free-spectral range (FSR) expansion [8], and our previous work on electro-optic logic-switching [9]. However, to the best of our knowledge, the resonance tuning characteristics by using free-carrier injection and their dependence on the feedback-waveguide-microring coupling have yet been investigated in detail.

Here, we report our experimental and theoretical study on the resonance characteristics of electrically reconfigurable silicon microring resonator-based filters with waveguide-coupled feedback. We tune the feedback phase and amplitude through the free-carrier plasma dispersion and absorption effect [10] by forward biasing a laterally embedded p-i-n diode. We show that the transmission resonances exhibit various attributes depending on the attenuated feedback coupling. We model our devices using scattering-matrix-based approach and find good agreement with the measurements.

2. Device principle

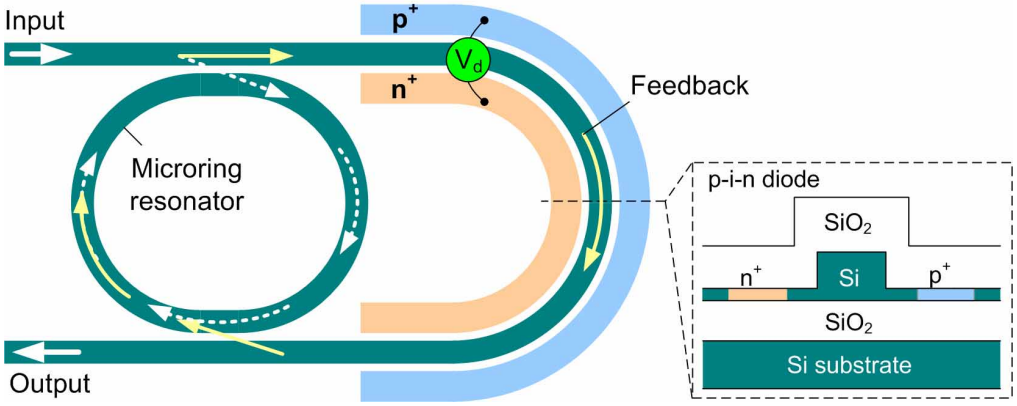

Fig. 1. Schematic of an electrically reconfigurable silicon microring resonator-based filter with waveguide-coupled feedback. Inset: cross-sectional view schematic of the lateral p-i-n diode embedded in the U-bend section. V_d: driving voltage.

Figure 1 shows the schematic of the electrically reconfigurable silicon microring resonator-based filter with waveguide-coupled feedback similar to our previous work [9]. The U-bend waveguide provides an external feedback to the microring resonator. The feedback phase and amplitude are electrically tunable by using an embedded lateral p-i-n diode. Inset illustrates the schematic cross-section of the p-i-n diode (along the dashed line).

Here, we outline the device principle. Input-coupled light field is partially coupled to the microring through the input-coupler and partially transmitted in the U-bend waveguide. The microring light field is partially out-coupled through the output-coupler (assumed symmetric to the input-coupler) and partially out-coupled through the input-coupler upon each round-trip. Whereas, the U-bend waveguide light field is partially feedback to the microring through the output-coupler and partially transmitted to the output-port. At the output-port, the interference between the microring light field and the U-bend waveguide light field yields the

#83924 - $15.00 USD Received 7 Jun 2007; revised 8 Jul 2007; accepted 9 Jul 2007; published 11 Jul 2007

transmission intensity. The phase-matching of such feedback-interfered round-trip field with the input-coupled field thus enables transmission intensity oscillations that are distinct from those of conventional waveguide-coupled microring resonators without external feedback. We can also regard the feedback-coupled microring as two coupled ring resonators, comprising the microring resonator and the feedback-loop ring resonator (composed of the feedback-waveguide, the left half-circle ring waveguide, and the two couplers waveguides). It is then conceivable to control the coupled ring resonances by only tuning the feedback-loop ring.

3. Model

We model our feedback-coupled microring resonator using scattering-matrix approach [11]. The steady-state relationship between the input and output electric-fields can be expressed as:

$$\begin{bmatrix} E_o \\ E_2 \end{bmatrix} = \begin{bmatrix} \tau e^{-i\varphi} & \kappa e^{-i(\varphi+\pi/2)} \\ \kappa e^{-i(\varphi+\pi/2)} & \tau e^{-i\varphi} \end{bmatrix} \begin{bmatrix} b\gamma e^{-i\phi} & 0 \\ 0 & a e^{-i\theta} \end{bmatrix} \begin{bmatrix} \tau e^{-i\varphi} & \kappa e^{-i(\varphi+\pi/2)} \\ \kappa e^{-i(\varphi+\pi/2)} & \tau e^{-i\varphi} \end{bmatrix} \begin{bmatrix} E_i \\ E_1 \end{bmatrix}, \quad (1)$$

where E_i and E_o are the input- and output-coupled electric-fields in the bus-waveguide, E_1 and E_2 are the electric-fields inside the microring just prior to the input-coupler and just after the output-coupler, κ and τ (real numbers) are the coupling and transmission coefficients of the symmetric input/output-couplers (for lossless coupling, $\tau^2 + \kappa^2 = 1$), φ is the transmission phase change of the couplers (for circular microring, $\varphi = 0$), a is the half-circular ring amplitude transmission factor, θ is the half-circular ring phase change, b is the feedback-waveguide amplitude transmission factor, γ is the amplitude transmission factor under free-carrier absorption ($\gamma = 1$ means no carrier injection), and $\phi = \phi_0 + \delta\phi$ is the feedback-waveguide phase change including a passive path-length phase change ϕ_0 and a carrier-injection induced phase shift $\delta\phi$. We note that ϕ_0 and θ are related with the feedback-waveguide length L_b and the half-circular ring length L_a as $\phi_0 = n_{eff} L_b (2\pi/\lambda)$ and $\theta = n_{eff} L_a (2\pi/\lambda)$, where n_{eff} is the waveguide effective refractive index and λ is the free-space wavelength. The two tuning parameters, $\delta\phi$ and γ, are related by free-carrier plasma dispersion effect [10]. Figure 2(a) depicts the modeling parameters.

The electric-fields E_1 and E_2 are related as follows,

$$E_1 = a e^{-i\theta} E_2 . \quad (2)$$

From Eqs. (1) and (2), we obtain the transmission as,

$$\frac{I_{out}}{I_{in}} = \left| \frac{E_o}{E_i} \right|^2 = \left| \frac{\tau^2 b\gamma e^{-i(\phi+2\varphi)} + \kappa^2 a e^{-i(\theta+2\varphi+\pi)} + a^2 b\gamma e^{-i(2\theta+4\varphi+\phi+\pi)}}{1 - [\tau^2 a^2 e^{-i(2\theta+2\varphi)} + \kappa^2 ab\gamma e^{-i(\theta+2\varphi+\phi+\pi)}]} \right|^2 . \quad (3)$$

We define the resonance phase-matching condition between the feedback-coupled round-trip field A and the input-coupled field at a point just prior to the input-coupler in terms of

$$A = |A| e^{-i\Phi} = \tau^2 a^2 e^{-i(2\theta+2\varphi)} + \kappa^2 ab\gamma e^{-i(\theta+2\varphi+\phi+\pi)} , \quad (4)$$

where Φ is the feedback-coupled round-trip phase change. Resonances occur at $\Phi = 2m\pi$ (m = 1, 2, 3…).

Figures 2(b) and 2(c) illustrate the physical meanings of the terms in Eqs. (3) and (4). In the numerator of I_{out}/I_{in} (Eq. (3) right-hand-side), the first term is the field transmission through only the feedback-waveguide (Fig. 2(b) red dashed line). The second term is the field transmission through only the half-ring waveguide (Fig. 2(b) blue dashed line). The third term represents the combined microring and feedback-waveguide field amplitude losses and round-trip phase shifts. In the denominator, the first significant term (also the first term in Eq.

#83924 - $15.00 USD Received 7 Jun 2007; revised 8 Jul 2007; accepted 9 Jul 2007; published 11 Jul 2007

(4)) is the microring field round-trip transmission with a round-trip phase change given by $2\theta+2\varphi$, corresponding to a round-trip path length of $2L_a+2L_c$, where L_c is the racetrack interaction length (Fig. 2(c) blue dashed line). The second significant term [also the second term in Eq. (4)] is the field round-trip transmission through the feedback-loop ring with a round-trip phase change given by $\theta+2\varphi+\phi+\pi$, corresponding to a round-trip path length of $L_a+2L_c+L_b$ (Fig. 2(c) red dashed line).

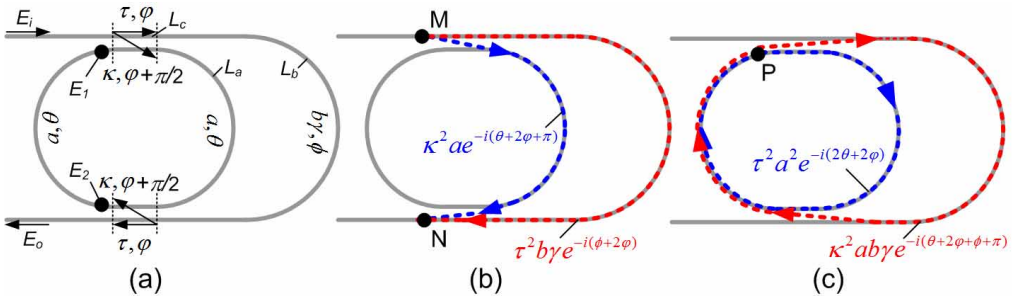

Fig. 2. (a). Modeling schematic. (b), (c) Physical interpretations of the terms in Eqs. (3) and (4). The corresponding terms of the electric-field transmissions through various paths are labelled. In (b), M: starting-point in the feedback-waveguide just prior to the input-coupler. N: ending-point in the feedback-waveguide just after the output-coupler. In (c), P: starting- and ending-points in the microring just prior to the input-coupler.

3.1 Two limiting cases

The microring and the feedback-loop ring each imposes a different round-trip phase change (i.e. $2\theta+2\varphi$ and $\theta+2\varphi+\phi+\pi$). Equation (4) suggests that in case $\tau^2a^2 >> \kappa^2ab\gamma$, the resonances can be approximated by the microring resonances given by $\Phi \approx 2\theta+2\varphi = 2m\pi$. Whereas in case $\tau^2a^2 << \kappa^2ab\gamma$, the resonances can be approximated by the feedback-loop ring resonances given by $\Phi \approx \theta+2\varphi+\phi+\pi = 2m\pi$. In general the resonances are given by the Φ phase-matching (Eq. (4)). Here, we further analyze the two limiting cases.

3.1.1 Microring approximation

For the ease of analysis, we assume that the transmission factors *a* and *b* are of the same order of magnitude, given both are largely determined by the waveguide propagation and bending losses. We then examine the microring approximation under two scenarios: (i) weak coupling $\tau^2 >> \kappa^2$, and (ii) excess carrier absorption loss $\gamma \approx 0$.

For weak coupling ($\tau^2 >> \kappa^2$) and under low injections ($\gamma \approx 1$), we simplify Eq. (3) as

$$\frac{I_{out}}{I_{in}} = b^2\gamma^2\left|\frac{\tau^2 - a^2e^{-i(2\theta+2\varphi)}}{1-\tau^2a^2e^{-i(2\theta+2\varphi)}}\right|^2, \tag{5}$$

which suggests an inverted Lorentzian resonance line shape. Equation (5) further suggests that critical coupling occurs at $\tau^2 = a^2$, meaning that null resonance transmission happens as the total electric-field transmission through both the input- and output-couplers balance the microring round-trip loss.

For excess carrier absorption loss ($\gamma \approx 0$), the feedback is largely attenuated and thereby the transmission is like the "drop" function as in a conventional add-drop filter. We simplify Eq. (3) as

$$\frac{I_{out}}{I_{in}} = a^2\kappa^4\left|\frac{1}{1-\tau^2a^2e^{-i(2\theta+2\varphi)}}\right|^2, \tag{6}$$

#83924 - $15.00 USD Received 7 Jun 2007; revised 8 Jul 2007; accepted 9 Jul 2007; published 11 Jul 2007

which suggests a Lorentzian resonance line shape.

3.1.2 Feedback-loop ring approximation

Here, the round-trip phase change Φ becomes an approximately linear function of the feedback phase change ϕ, suggesting that the resonance wavelength approximately linearly depends on ϕ. The feedback-loop ring approximation is satisfied under strong coupling $\tau^2 << \kappa^2$ and low carrier absorption loss $\gamma \approx 1$. We simplify Eq. (3) as

$$\frac{I_{out}}{I_{in}} = a^2 \left| \frac{\kappa^2 - ab\gamma e^{-i(\theta+2\varphi+\phi+\pi)}}{1-\kappa^2 ab\gamma e^{-i(\theta+2\varphi+\phi+\pi)}} \right|^2, \tag{7}$$

which suggests an inverted Lorentzian resonance line shape. Equation (7) further suggests that critical coupling happens at $\kappa^2 = ab\gamma$, meaning that null resonance transmission happens as the total coupled electric-field through both the input- and output-couplers balances the total field feedback-loop ring round-trip loss.

3.2 Phase-matched feedback

The transmission according to Eq. (3) suggests that the resonance ER and line shape in general oscillates among the resonances. In order to attain a nearly uniform resonance ER and line shape distribution, we can design the feedback-waveguide length L_b such that every resonance sees nearly the same feedback phase and amplitude. We refer to this condition as phase-matched feedback.

Here, we show that each resonance exhibits the same transmission intensity in case the relative feedback phase change $\Delta\phi \equiv \phi - \theta$ satisfies

$$\Delta\phi(\lambda_m) = 2n_m\pi + c, \tag{8}$$

where λ_m is the mth resonance wavelength, n_m is an integer, and c is a constant phase angle.

From Eqs. (4) and (8), we express field A upon phase-matched feedback as

$$A = e^{-i(2\theta+2\varphi)}[\tau^2 a^2 - \kappa^2 ab\gamma e^{-ic}]. \tag{9}$$

The term in the square bracket is a constant complex number (independent of wavelength), and thus we rewrite it as $\tau^2 a^2 - \kappa^2 ab\gamma e^{-ic} = |A| e^{i\Phi_c}$. The resonance condition becomes

$$\Phi = 2\theta + 2\varphi - \Phi_c = 2m\pi. \tag{10}$$

From Eq. (3) and using Eqs. (8) and (10), we express the transmission at λ_m as

$$\left(\frac{I_{out}}{I_{in}}\right)_{\lambda_m} = \left| \frac{\tau^2 b\gamma e^{-ic} - \kappa^2 a - a^2 b\gamma e^{-i\Phi_c} e^{-ic}}{1 - e^{-i\Phi_c}[\tau^2 a^2 - \kappa^2 ab\gamma e^{-ic}]} \right|^2. \tag{11}$$

The right-hand side of Eq. (11) is independent of resonance mode number m. Hence, Eq. (11) suggests that the transmission is identical at each resonance wavelength upon satisfying the phase-matched feedback condition.

In order to determine the proper L_b and L_a for phase-matched feedback, we express $\Delta\phi$ as

$$\Delta\phi(\lambda) = n_{eff} \frac{2\pi}{\lambda}(L_b - L_a) + \delta\phi. \tag{12}$$

We note that $\delta\phi << n_{eff}\, 2\pi(L_b - L_a)/\lambda$. It is thus possible to choose a particular $(L_b - L_a)$ such that Eq. (8) is approximately satisfied for consecutive resonance wavelengths over a narrow spectral range.

#83924 - $15.00 USD Received 7 Jun 2007; revised 8 Jul 2007; accepted 9 Jul 2007; published 11 Jul 2007

We can write the resonance condition in general form as,

$$n_{eff} L_{res} = m\lambda_m , \tag{13}$$

where L_{res} is the effective round-trip length for resonance phase matching.

From Eqs. (12) and (13) and considering $\Delta\phi(\lambda_{m+1}) - \Delta\phi(\lambda_m) = 2n\pi$, where n is an integer, we obtain the phase-matched feedback condition as

$$L_b - L_a = nL_{res} \quad (\text{n} = 1, 2, 3\ldots). \tag{14}$$

For devices close to the microring approximation, $L_{res} \approx 2(L_a+L_c)$, we can choose L_b values to satisfy Eq. (14) as follows

$$L_b \approx 2n(L_a + L_c) + L_a . \tag{15}$$

In case $n = 1$, we have $L_b + L_a + 2L_c \approx 2(2L_a + 2L_c)$, which means that the feedback-loop ring round-trip length needs to be approximately twice the microring round-trip length for nearly phase-matched feedback. However, for devices close to the feedback-loop ring approximation, $L_{res} \approx L_b + L_a + 2L_c > L_b - L_a$, there are no L_b's to satisfy Eq. (14).

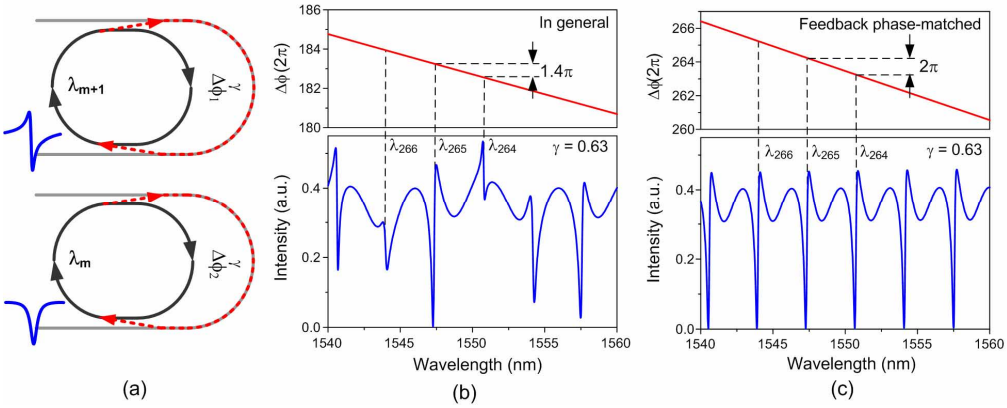

Fig. 3. (a). Illustration of the resonance-dependent line shapes in general cases. Resonances at wavelengths λ_{m+1} and λ_m see different feedback phase values $\Delta\phi_{m+1}$ and $\Delta\phi_m$. (b) and (c) Modeled feedback phase $\Delta\phi(\lambda)$ and the corresponding transmission spectra with (b) $\Delta\phi(\lambda_{m+1})$ - $\Delta\phi(\lambda_m) \approx 1.4\pi$, and (c) $\Delta\phi(\lambda_{m+1})$ - $\Delta\phi(\lambda_m) \approx 2\pi$.

Figures 3(a) illustrates schematically the resonance-dependent line shapes for two adjacent resonance wavelengths λ_{m+1} and λ_m. As λ_{m+1} and λ_m in general see different $\Delta\phi$ values that do not satisfy Eq. (8), the resonance line shape varies. Figure 3(b) shows the modeled $\Delta\phi(\lambda)$ for an arbitrary $(L_b - L_a)$ and the corresponding transmission spectrum using Eq. (3). We choose the following modeling parameters: L_a = 25 μm, L_b = 200 μm, L_c = 10 μm, τ^2 = 0.9, n_{eff} = 2.33, a = 0.92, b = 0.92, and γ = 0.63. Here $\Delta\phi(\lambda_{m+1}) - \Delta\phi(\lambda_m) \approx 1.4\pi$ and thus different resonances exhibit different line shapes. Figure 3(c) shows the modeled $\Delta\phi(\lambda)$ for an $(L_b - L_a)$ that satisfies Eq. (15) and the corresponding transmission spectrum using Eq. (3). We adopt L_b = 254 μm and the other parameters are identical to those in Fig. 3(b). In this case, $\Delta\phi(\lambda_{m+1}) - \Delta\phi(\lambda_m) \approx 2\pi$, and the modeling shows that not only the resonance intensity but also the resonance line shape are nearly uniformly distributed in the spectrum. The uniformity spans over multiple FSRs (10's nm).

#83924 - $15.00 USD Received 7 Jun 2007; revised 8 Jul 2007; accepted 9 Jul 2007; published 11 Jul 2007

4. Device design and fabrication

We design three different devices which address different waveguide-microring coupling regimes and different feedback path lengths. Device (I) comprises a circular microring of radius of 25 μm, L_b = 180 μm, and an integrated p-i-n diode spanning 130 μm. Device (II) comprises a circular microring of radius of 25 μm, L_b = 230 μm, and an integrated p-i-n diode spanning 180 μm. Device (III) comprises a racetrack microring with a curved waveguide radius of 25 μm and a straight interaction length L_c = 10 μm, L_b = 230 μm, and an integrated p-i-n diode spanning 130 μm. All the devices have the same design parameters except those specified above. For devices (I) and (II), we determine the power coupling ratio κ^2 is ~10% between the straight bus waveguide and the curved ring waveguide (according to numerical beam-propagation method (BPM) simulations). This suggests that the circular microring is weakly coupled with the feedback-waveguide. For device (III), we determine κ^2 is ~50% between the straight bus waveguide and the straight waveguide section of the racetrack. This suggests that the racetrack microring is strongly coupled with the feedback-waveguide.

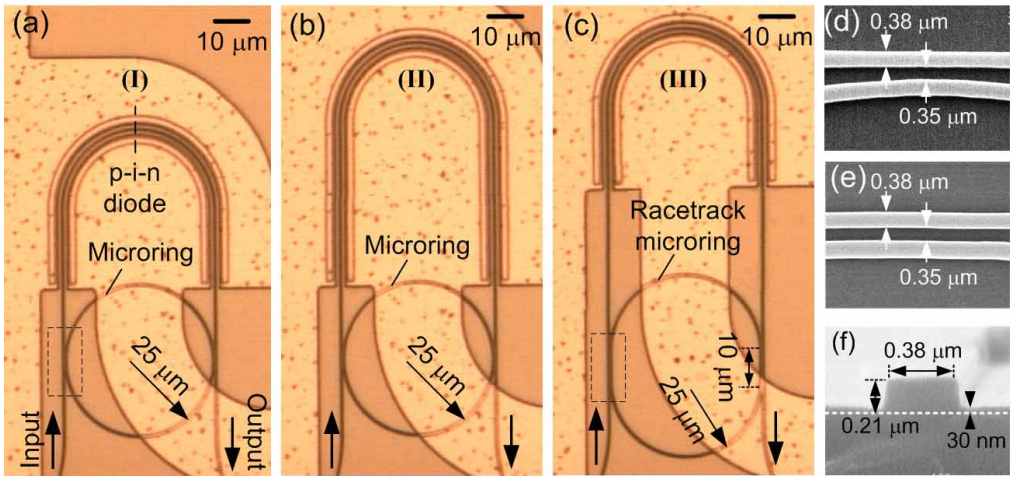

Fig. 4. (a).-4(c). Optical micrographs of the three fabricated devices (I), (II), and (III). (d) and (e) Zoom-in view SEMs of (d) the waveguide-circular-microring coupling region, and (e) the waveguide-racetrack-microring coupling region without oxide upper-cladding. (f) Cross-sectional view SEM of the single-mode waveguide without oxide upper-cladding.

We fabricate our devices on silicon-on-insulator (SOI) wafers using standard silicon microelectronics processes including photolithography (i-line, 365 nm), reactive ion etching, and ion implantation similar to our previous work [12]. Figures 4(a)-4(c) show the top-view optical micrographs of three typical devices (I), (II), and (III) fabricated on a SOI substrate (with a 0.21-μm device layer on a 2-μm buried-oxide layer). Aluminum pads are connected to the two electrodes of the embedded p-i-n diode for each device. The n^+- and p^+-doped regions underneath are 3-μm wide, and each has a separation of 0.5 μm from the waveguide sidewall. Figures 4(d) and 4(e) show the zoom-in-view scanning electron micrographs (SEMs) of the waveguide-circular-microring and waveguide-racetrack-microring coupling regions before cladding the entire device with an insulating oxide layer. Both the single-mode bus waveguide and the microring waveguide widths are ~0.38 μm, and the gap separations are ~0.35 μm. Figure 4(f) shows the cross-sectional view SEM of the waveguide. The waveguide height is 0.21 μm with an etched depth of 0.18 μm.

#83924 - $15.00 USD Received 7 Jun 2007; revised 8 Jul 2007; accepted 9 Jul 2007; published 11 Jul 2007

5. Results

We first examine device (I) transmission characteristics under low injection levels ($V_d \leq 1$ V), where the free-carrier absorption loss is small. Figures 5(a)-5(c) show the measured and modeled TE-polarized (electric field parallel to the chip) single-mode transmission spectra of device (I) under forward biases of V_d = 0 V, 0.9 V, and 1.0 V. The modeled transmission spectra (using Eq. (3)) assume a = 0.96 and b = 0.95. We choose κ= 0.34 (satisfying $\kappa^2 << \tau^2$). We determine the wavelength-dependent feedback phase ϕ_0 by BPM simulation (thus incorporating the waveguide dispersion). We then choose $\delta\phi$ and γ values (labeled in the Figs.) to best-fit the measured transmission spectra. In particular, we choose $\delta\phi$ = 0 and γ= 1 for V_d = 0 V, and γ remains ≈1 for the small V_d's. We also assume $\delta\phi$ and γ are independent to wavelength within the spectral range of interest. The modeled spectra show good agreement with the experimental results.

We notate three resonances as resonances A, B, and C. The FSR is ~3.8 nm, which is consistent with the microring resonator round-trip path length. As the microring resonator is weakly coupled with the feedback-waveguide, the device is close to the microring approximation and the resonances are mainly given by the microring resonator.

We observe that the resonances ER and Q values display quasi-periodic oscillations over multiple FSRs. Resonance A exhibits the maximum Q of ~10^4. Moreover, while the resonance wavelengths are almost fixed within ~0.05-nm shift under the three V_d's, the ER values vary significantly (most pronounced for resonance C) yet with only slight variations in the Q values. Thus, we see that in the case of low injection levels with low carrier absorption loss, V_d (essentially $\delta\phi$) primarily controls the resonance ER. We attribute the background intensity fluctuations in the measured spectra to modulations due to the U-bend waveguide end-face back-reflections.

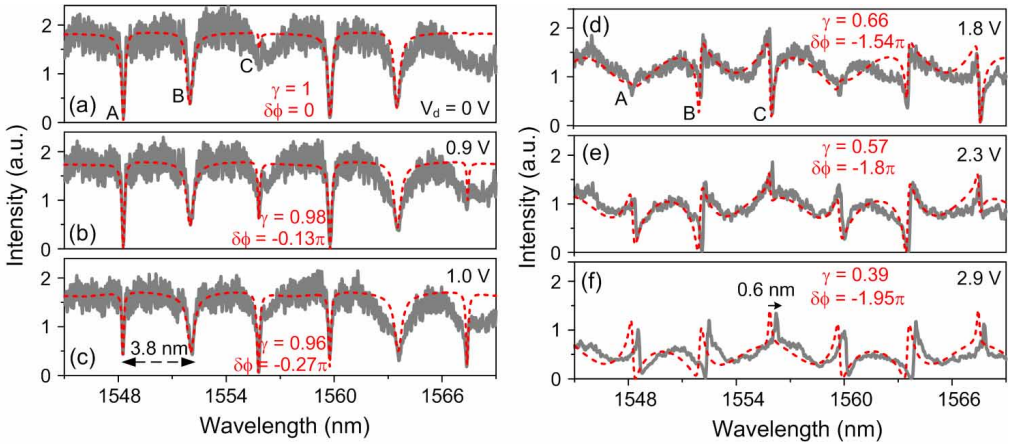

Fig. 5. (a)-(c) Measured (solid grey lines) and modeled (dashed red lines) TE-polarized transmission spectra of device (I) upon low injection levels with bias voltages of V_d = (a) 0 V, (b) 0.9 V, and (c) 1.0 V. (d)-(f) Measured (solid grey lines) and modeled (dashed red lines) TE-polarized transmission spectra of device (I) upon high injection levels with bias voltages of V_d = (a) 1.8 V, (b) 2.3 V, and (c) 2.9 V.

We also examine device (I) transmission characteristics upon high injection levels, in which the free-carrier absorption loss becomes significant. Figures 5(d)-5(f) show the measured and modeled TE-polarized single-mode transmission spectra of device (I) under three high forward biases of V_d = 1.8 V, 2.3 V, and 2.9 V. In the modeling we again choose $\delta\phi$ and γ values (labeled in the Figs.) to best-fit the measured transmission spectra, while other modeling parameters remain the same as those in the low injection cases. Interestingly, we find asymmetric resonance line shapes [12] (Fano resonances [13]) quasi-periodically appear

#83924 - $15.00 USD Received 7 Jun 2007; revised 8 Jul 2007; accepted 9 Jul 2007; published 11 Jul 2007

over a wide range of wavelength. Besides, the Fano line shapes evolve with V_d. Thus, we find that upon certain high injections to the feedback-waveguide, the resulting phase shifts and attenuations can controllably tune the asymmetric resonance line shapes. We also observe that upon high V_d, the measured resonance spectra display a slight redshift relative to those at low V_d (~0.6 nm redshift at V_d = 2.9 V), which we attribute to the thermo-optic effect in silicon (estimated ~5°C temperature rise). The measured transmission spectra also display insertion loss increases with V_d, which is consistent with an increased free-carrier absorption loss. We also note that the measured transmission intensity fluctuations with the high V_d are less pronounced than those with the low V_d, which again can be attributed to the enhanced free-carrier absorption loss in the U-bend waveguide.

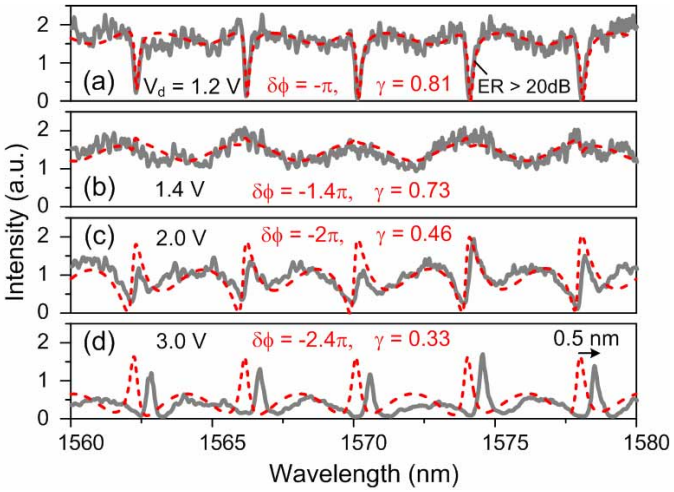

Fig. 6. (a).-(d). Measured (solid grey lines) and modeled (dashed red lines) TE-polarized transmission spectra of device (II) under various bias voltages of V_d = (a) 1.2 V, (b) 1.4 V, (c) 2.0 V, and (d) 3.0 V.

Figures 6(a)-6(d) show the measured and modeled TE-polarized transmission spectra of device (II) under various bias voltages of V_d = 1.2 V, 1.4 V, 2.0 V, and 3.0 V. Except for the $\delta\phi$ and γ values labeled in the Figs., the modeling parameters are the same as those in device (I). The resonances under the different V_d's exhibit four main characteristics: resonance dips with ER > 20 dB [Fig. 6(a)], modulated all-pass transmission [Fig. 6(b)], asymmetric Fano line shapes [Fig. 6(c)], and resonance peaks (Fig. 6(d)). Like device (I), device (II) displays an FSR of ~3.8 nm, which is consistent with the microring round-trip length. This suggests that the resonances are also mainly given by the microring resonator. Yet, unlike device (I), device (II) displays nearly uniform resonance line shapes over multiple FSRs. This is because device (II) design parameters (see Sec. 4) satisfy the phase-matched feedback condition (Eq. (15) with n = 1).

Figures 7(a)-7(d) show the measured and modeled TE-polarized multimode transmission spectra of device (III) under various bias voltages of V_d = 0.7 V (sub-threshold), 1.5 V, 2.0 V, and 2.9 V. We choose κ = 0.7 in the modeling while other parameters are the same as those in device (I). As $\kappa^2 \approx \tau^2$, the microring approximation no longer holds. Instead, we discern two sets of resonances that can be attributed to the mutual coupling between the microring and the feedback-loop ring. We denote two resonance modes D and E [Figs. 7(b)-7(d)], which display different ER values and line shapes under various bias voltages. We remark that although device (III) is designed to satisfy the phase-matched feedback condition (Eq. (15) with n = 1), the significant mutual coupling violates the microring approximation and thus forbids the resonance line shapes to remain uniform across multiple FSRs.

#83924 - $15.00 USD Received 7 Jun 2007; revised 8 Jul 2007; accepted 9 Jul 2007; published 11 Jul 2007

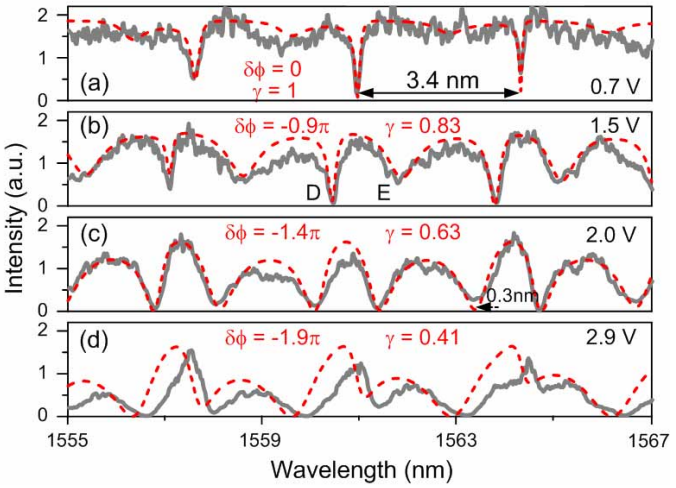

Fig. 7. Measured (solid grey lines) and modeled (dashed red lines) TE-polarized transmission spectra of device (III) under various bias voltages of V_d = (a) 0.7 V, (b) 1.5 V, (c) 2.0 V, and (d) 2.9 V.

We also use our model to analyze a device in strong-coupling regime. We consider feedback-coupling to a racetrack microring that has an interaction length of ~20 μm and a $\kappa \approx$ 0.94. We choose L_b = 274 μm satisfying Eq. (15) with n = 1. Figures 8(a)-8(e) show the modeled transmission spectra and their evolution under various attenuated feedback conditions.

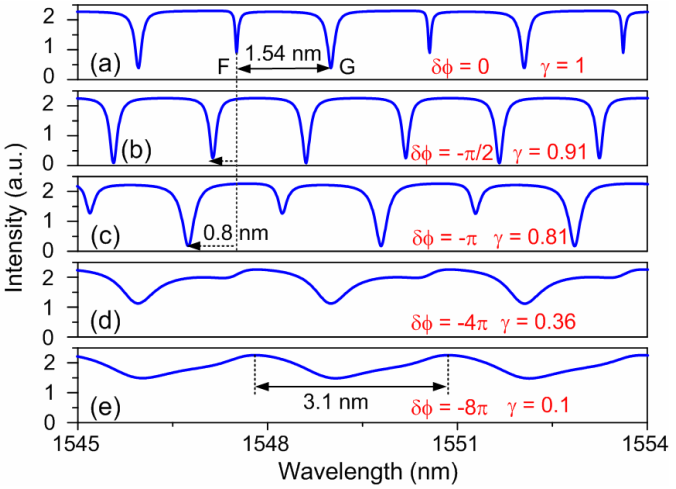

Fig. 8. (a).-(e). Modeled transmission spectra under various attenuated feedback conditions for a racetrack microring device with strong coupling ($\kappa \approx$ 0.94).

Under low attenuations (see Figs. 8(a)-8(c)), we find that the modeled resonances are mainly given by the feedback-loop ring. The modeled FSR of 1.54 nm is consistent with the feedback-loop ring path length of 394 μm, suggesting that the resonances are close to the feedback-loop ring approximation. We also discern resonance wavelength blueshifts by ~0.8 nm with $\delta\phi = -\pi$. This wavelength tuning with $\delta\phi$ is again consistent with the feedback-loop ring approximation. In fact, among the four device configurations studied here, the feedback-

#83924 - $15.00 USD Received 7 Jun 2007; revised 8 Jul 2007; accepted 9 Jul 2007; published 11 Jul 2007

loop ring approximation under strong coupling and low attenuation exhibits the most efficient wavelength tuning by phase-shifting the feedback-waveguide. The modeling also shows that the resonance ER and line shape vary with $\delta\phi$ and γ, yet the resonance ER and line shape are non-uniform across the spectrum as the feedback-loop ring approximation does not have the phase-matched feedback condition.

Under high attenuations (Figs. 8(d) and 8(e)), however, we see that the modeled resonances are essentially attenuated microring resonances. The modeled FSR is expanded to 3.1 nm, which is consistent with the microring round-trip path length of 197 μm. This suggests that the strongly attenuated feedback, regardless of its strong coupling, yields attenuated microring resonances.

6. Conclusion

In conclusion, we have experimentally demonstrated an electrically reconfigurable silicon microring filter comprising a feedback-waveguide-coupled microring resonator with an injection-type p-i-n diode integrated to the feedback-waveguide. We have investigated the resonance tuning characteristics under various free-carrier injection levels for devices with various coupling strengths and feedback-waveguide lengths. Both experiments and scattering-matrix-based modeling show that the resonance attributes (wavelengths, extinction ratios, and line shapes) are strongly dependent on the feedback coupling and can be controllably tuned by means of varying the feedback phase and amplitude through carrier injection to the feedback-waveguide. We have also demonstrated transmission spectra with nearly uniform resonance line shapes over multiple free-spectral ranges, by means of nearly phase-matching the feedback and the microring fields for devices with weak coupling to the feedback-waveguide. With the demonstrated flexibility in controlling the resonance attributes, we believe that such feedback-coupled microring filters can be another useful component in the silicon photonics tools box.

Acknowledgment

The research was substantially supported by a grant from the Research Grants Council of The Hong Kong Special Administrative Region, China (Project No. 618505).

#83924 - $15.00 USD Received 7 Jun 2007; revised 8 Jul 2007; accepted 9 Jul 2007; published 11 Jul 2007